This article has been accepted for publication in IEEE Transactions on Transportation Electrification. This is the author's version which has not been fully edited and content may change prior to final publication. Citation information: DOI 10.1109/TTE.2025.3528227

High-Frequency Power Loss Investigation of Pavement Materials in Roadway Inductive Charging System

Zilong Zheng, *Student Member, IEEE*, Xiao Chen, Yao Wang, Hua Zhang, Hao Wang, Fei Lu, *Member, IEEE*

***Abstract*- The rapid advancement of electric vehicles (EVs) offers a significant reduction in carbon emissions by replacing fossil fuels with more sustainable energy sources. This paper studies wireless charging technology for EVs, focusing on high-frequency power losses. It presents an experimental investigation into the inductive power transfer (IPT) system's efficiency under various pavement materials (specifically, asphalt and concrete), revealing significant power losses due to material electromagnetic properties. This research provides insights into optimizing IPT system design through empirical analysis of power losses across different frequencies and magnetic flux densities. Three main contributions are highlighted: quantifying power loss density, developing an empirical equation for magnetic losses, and identifying the significant impact of pavement materials on overall system efficiency. A 17.8 kW IPT system is implemented to measure and validate the power losses in pavement materials. This research underscores the critical need for interdisciplinary approaches to enhance the feasibility of IPT systems for future autonomous and smart city applications.**

***Index Terms*—Inductive power transfer (IPT), power loss, road pavement material, wireless power transfer (WPT), dynamic wireless power transfer (DWPT)**

I. Introduction

As an effective way to reduce fossil fuel consumption, the development of electric vehicles (EVs) has advanced rapidly over the past decade, offering an eco-friendlier transportation alternative to mitigate carbon emissions and combat global warming. Nonetheless, EV charging still predominantly relies on traditional conductive charging methods. Recently, there has been a growing focus on leveraging wireless power transfer (WPT) technology for EV charging to address the limitations and inconvenience associated with traditional conductive charging methods. Moreover, WPT technology can facilitate the integration of intelligent transportation systems (ITS), vehicle-to-grid (V2G), and various vehicle-to-vehicle (V2V) applications [1]-[3], paving the way for a truly sustainable and fully autonomous future.

In terms of charging EVs wirelessly, there are two primary WPT options: stationary wireless power transfer (SWPT) and dynamic wireless power transfer (DWPT) [4], [5]. Both methods predominantly utilize compensated inductive power transfer (IPT) technology. DWPT offers enhanced flexibility and convenience by enabling on-the-go charging, making it particularly promising for the future of transportation and the integration into smart city infrastructures.

This approach eliminates the need for vehicles to stop for charging by providing continuous power transfer while in motion. The potential of DWPT lies in its ability to reduce the burden on the vehicle's battery by supplying consistent energy along the travel route, effectively addressing both range anxiety and battery capacity limitations [6], [7]. Such a system is particularly effective in reducing battery size when deployed on dedicated routes—such as public transit systems or specific highways—where vehicles have consistent access to wireless charging infrastructure. This deployment enables significant reductions in battery size [8], [9]-[11]. In such controlled environments, batteries serve primarily as backup or for short-distance travel, as continuous wireless power minimizes the vehicle's reliance on stored energy. Consequently, this approach reduces vehicle weight and cost, making DWPT an attractive solution for electric vehicle operations on fixed routes.

This wireless charging process, as shown in Fig. 1(a) eliminates the need for human involvement in handling the high-voltage charging cable, thereby reducing the risk of physical injury and mental stress associated with remembering and operating the high-voltage charging cable involved in the traditional plug-in charging process [12]-[15]. As a result, it provides a safer, more convenient, and robust energy transfer solution to meet the needs of ITS [16]-[18].

While DWPT systems offer significant benefits in providing continuous power to the vehicle while it is in motion, the mounting position of the ground assembly (GA), which

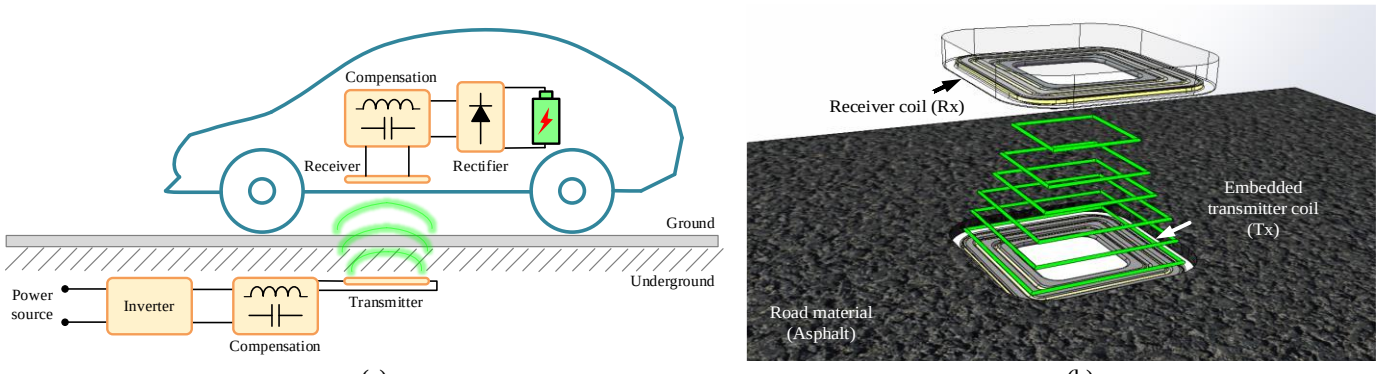

Fig. 1. Structure of a WPT system illustrating the importance of investigating the pavement material impacts on the WPT system efficiency. (a) Road-embedded inductive charging system concept. (b) Buried mounting GA coil, showing interference with asphalt.

This article has been accepted for publication in IEEE Transactions on Transportation Electrification. This is the author's version which has not been fully edited and content may change prior to final publication. Citation information: DOI 10.1109/TTE.2025.3528227

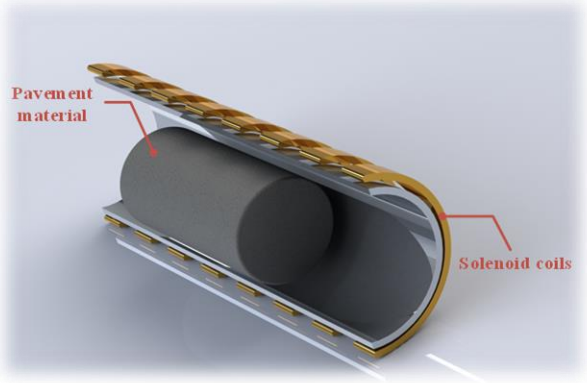

Fig. 2. Structure of a solenoid coil to generate an evenly distributed magnetic field environment for pavement material testing.

includes the GA coil, is an important consideration. The current SAE J2954 standard primarily focuses on above-ground mounting of the GA [19], due to its ease of installation, maintenance, and alignment. However, future versions of the standard and SAE J2954/2 is currently classified as a Technical Information Report (TIR) for heavy-duty vehicles, are expected to explore buried mounting configurations as a focus shown in Fig. 1(b), particularly for dynamic wireless power transfer (DWPT) systems [20], [21]. Embedding the GA within the road pavement could provide enhanced protection for internal components and support seamless vehicle movement [22]-[24], though specific technical and safety requirements are still under development. This evolving approach will play a crucial role in further optimizing DWPT systems for both public transit and highway applications, where consistent and reliable power transfer is essential. During the charging process, these materials can lead to additional power loss and heat generation [25], [26] due to their distinct electromagnetic and physical characteristics. However, understanding the exact cause of power loss from various pavement materials is a complex process which requires interdisciplinary collaboration.

In this paper, an experimental investigation is conducted to directly measure and observe the power loss phenomenon for various concrete and asphalt pavement materials. There are 4 different concrete materials and 3 different asphalt materials tested under an evenly distributed magnetic field, generated by a resonant LCR circuit using a solenoid coil, shown in Fig. 2.

Furthermore, the selected concrete and asphalt materials based on the results of the power loss experiment are tested again in an IPT prototype under various power levels up to 17.833 kW at frequency f= 85 kHz. These testing benchmarks are conducted based on the Society of Automotive Engineers (SAE) J2954 standards for EVs and EV Supply Equipment (EVSE) that published in October 2020 [27], [28]. Since the standardization of J2954, there is substantial amount of research aimed at improving efficiency within the design of IPT system themselves. However, there is a wide gap in the research related to analyzing the power loss attributed to different pavement materials as the energy transfer medium and how they affect the efficiency and power level of an IPT system when the transmitter is embedded in pavement materials.

Several studies have highlighted the critical role of material selection and its impact on the performance of DWPT systems, each approaching the topic from distinct disciplinary perspectives. Chen et al. investigated the dielectric properties of pavement materials and their impact on the efficiency of IPT systems from a civil engineering perspective, revealing that moisture content significantly affects power loss and overall efficiency [28]. Cirimele et al. emphasized the influence of the electromagnetic parameters of concrete and the geometrical configuration of road-embedded coils on the performance of WPT systems, demonstrating that these factors can lead to unexpected electromagnetic interactions that alter the system's inductive behavior [29]. Amirpour et al. explored the thermal and electromagnetic performance of magnetizable concrete composites from a thermal engineering perspective, showing that appropriate material selection and configuration can mitigate power losses by managing thermal effects [30]. Tavakoli et al. examined how the incorporation of new roadway construction materials can enhance magnetic properties and reduce electromagnetic interference, providing insights for optimizing material choices in DWPT systems [31]. Collectively, these studies underscore the importance of comprehensive pavement material characterization and selection for achieving efficient and reliable DWPT systems.

Throughout this study, significant power losses are observed in several scenarios. Therefore, it is critical to investigate and quantify the power loss associated with different pavement materials. Understanding how different pavement materials impact the power loss of an IPT system could lead to

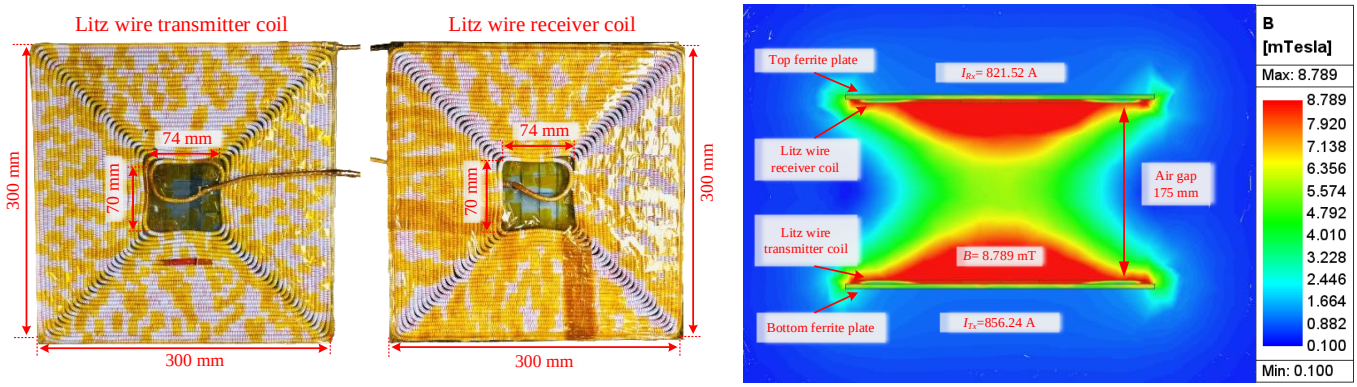

(a) (b)

Fig. 3. Planar coil prototypes to realize high-power wireless charging testing and study the magnetic field distribution when transfer 17.8 kW high power. (a) Implemented planar coil prototypes to achieve wireless charging. (b) Maxwell-simulated magnetic field. distribution of planar coils.

improvements in the design of the entire charging system for both SWPT and DWPT.

Moreover, these findings highlight strategies for selecting pavement materials in road construction, thereby improving the overall performance and feasibility of WPT technology. This is particularly relevant for the integration into smart city infrastructures and supporting fully autonomous driving.

There are 3 main contributions in this research: 1) Obtained and analyzed the power loss density D (kW/m^3) for both concrete and asphalt materials under different frequencies f from 50 kHz to 120 kHz with magnetic flux density B from 0.71 mT with 0.34 kA to 7.02 mT with 3.34 kA. 2) Leveraging the extensive experimental data collected, an empirical equation is developed based on the Steinmetz Equation to quantify the relationship for each tested pavement material for the various magnetic losses, system frequency f, and magnetic flux density B. 3) Observed significant power loss density for the tested pavement materials under a proposed IPT system which its power level reaches almost 18 kW.

II. Quantification of Pavement Material's Power Loss Under Uniform Magnetic Field

A. The Design of Uniform Magnetic Field

An example of a unipolar square coil is shown in Fig. 3, in which Fig. 3(a) presents the planar coil structure. Fig. 3(b) shows the generated magnetic fields that exhibit a non-uniform distribution, with variations in magnetic flux density across different regions. The higher magnetic flux density is represented by red and orange colors, while lower magnetic flux density is indicated by green and blue colors. This non-uniformity, inherent to the planar coil geometry, complicates the analysis of power loss for various pavement materials, as the power loss is influenced by the local magnetic flux density B and its alternating frequency f. Therefore, it is necessary to produce a uniform magnetic field to investigate the relationship between these key factors. It can be achieved by utilizing a solenoid coil to generate an evenly distributed magnetic field within its internal space as shown in Fig. 4.

Based on Ampere's Circuital Law, the magnetic field intensity H, integrated along a closed rectangular path represented as l_{abcd} is given by Equation (1). In this equation, μ_0 represents the magnetic permeability of free space ($4\pi\times10^{-7}$ H/m), μ_r is the relative magnetic permeability of non-ferromagnetic materials, such as concrete or asphalt, and μ_m is the material permeability [29]. The number of turns N of the coil is that the path encircles, and I is the current enclosed by the path. The total magnetic field intensity along l_{abcd} can be expressed as the sum of the magnetic field components along the path, denoted as H_{ab}, H_{bc}, H_{cd} and H_{da}. When the length l is significantly greater than its diameter, the component H_{ab} dominates, and the contributions from H_{bc}, H_{cd} and H_{da}, can be neglected, as shown in Equation (2).

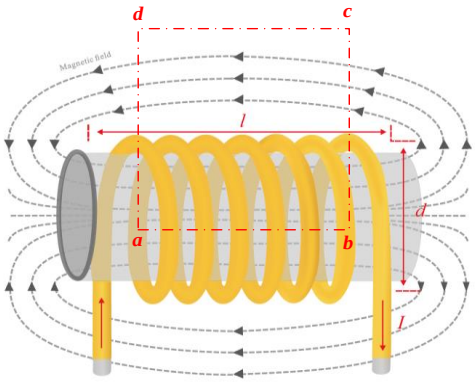

Fig. 4. A solenoid coil structure to create an internal uniform magnetic field environment for further pavement material testing.

$$\begin{cases} \int_{l_{abcd}} H\cdot dl = NI \\ \int_{l_{abcd}} H\cdot dl = \int_{l_{ab}} H_{ab}dl + \int_{l_{bc}} H_{bc}dl + \int_{l_{cd}} H_{cd}dl + \int_{l_{da}} H_{da}dl \end{cases} \tag{1}$$

$$H_{abcd} = H_{ab} = \frac{NI}{l_{ab}} \tag{2}$$

$$\begin{cases} B_m = \mu_m H = \mu_0\mu_r H \\ B_m = \mu_0 H \end{cases} \tag{3}$$

$$B_{abcd} = \mu_0\mu_r H_{ab} = \mu_0 NI/l_{ab} \tag{4}$$

The relative magnetic permeability μ_r of non-ferromagnetic materials, such as concrete or asphalt, is μ_r= 1, shown in Equation (3). Therefore, the magnetic flux density B_{abcd} can be determined by Equation (4).

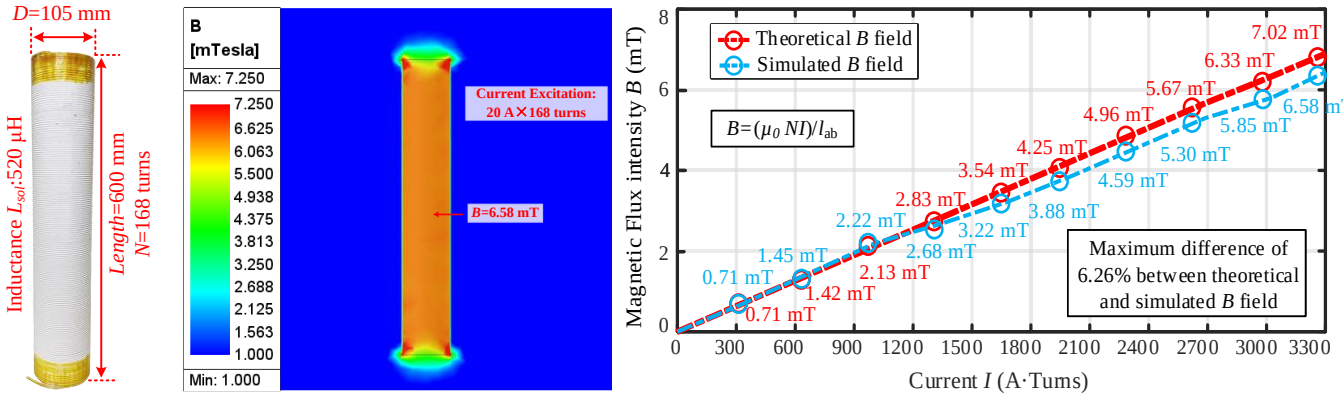

(a) (b) (c)

Fig. 5. The statistical derivation of the impact parameters in an empirical equation to model the power loss density D of concrete cement PC at various magnetic flux densities (0-5 mT) and frequencies (0-120 kHz). (a) Coil dimensions. (b) Maxwell-simulated magnetic field. (c) Comparison of simulated and theoretical B fields by equations (1)-(3)

B. *Experimental Validation of Pavement Material Power Loss in Different Uniform Magnetic Fields*

During the test process, the cylinder structure pavement material specimens are placed in the middle section of the solenoid coil inside of it to ensure that a uniform magnetic field environment is provided.

Detailed parameters of the constructed solenoid coil are shown in Fig. 5(a). It has a length l of 600 mm, a diameter d of 105 mm, and an inductance L_{sol} of 520 μH. It contains 168 turns of litz wire consisting of 0.04 mm individual strands with a total gauge equivalent to AWG 46 wire.

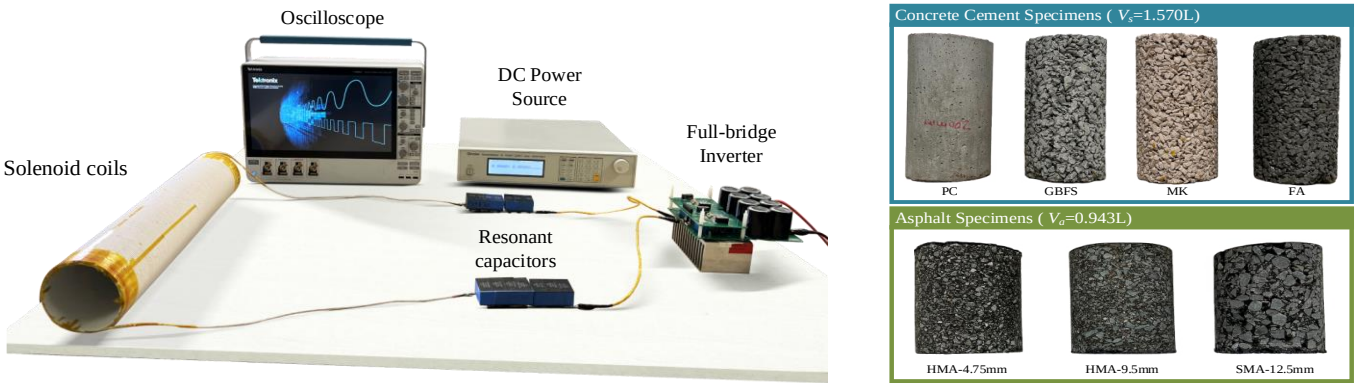

(a) (b)

Fig. 6. Testing platform to generate uniform magnetic fields in a long solenoid coil to measure power loss in cylinder-shape pavement materials. (a) *LCR* based testing platform including a solenoid coil and its resonant circuit. (b) Seven tested pavement materials corresponding to Table 1.

Fig. 5(c) shows both the theoretical and simulated magnetic flux densities B produced by the constructed solenoid coil with different excitation current I. It shows high consistency between the simulated and theoretical magnetic flux density B, which validates the proposed method of creating uniform magnetic field. For example, with the excitation current I= 20 A, the simulated magnetic flux density B is 6.58 mT, that is only 6.26% different from the theoretical B=7.02 mT.

The voltage supplied by the dc power source; the conductive parasitic resistance of this circuit is R_c. The power loss induced by the pavement material is equivalent to a resistance R_M. A current I was regulated by V_s within a range of 0 A to 20 A (RMS). In this study, the switching frequency varied from 50 kHz to 120 kHz. At each frequency, the capacitance is adjusted to ensure the circuit is in resonance, supplying a sinusoidal current.

The selection of the tested frequency range is driven by several key factors grounded in real-world WPT developments and research objectives. Firstly, exploring higher frequencies, especially around 100 kHz, is essential for high-power and DWPT applications, such as heavy-duty electric vehicles, which demand greater power transfer efficiency and misalignment tolerance than standard light-duty systems operating at 85 kHz. The SAE J2954/2 TIR for heavy-duty vehicles allows for flexible frequency selection, making this range ideal for accommodating larger air gaps and improving overall performance [32]. Secondly, this approach ensures the system's flexibility and compliance with global regulatory standards, as different regions have varying regulations for wireless frequency use [33]. In summary, testing the 50 kHz to 120 kHz range allows us to comprehensively assess WPT system performance, security, and compliance, contributing to the development of robust, efficient, and adaptable wireless charging technologies for diverse applications [34].

During the experimental tests, the total power loss for the entire *LCR* circuit is measured across various transfer mediums: air, 4 different concrete cement specimens, and 3 different asphalt specimens, under various magnetic flux densities B and frequencies f. Based on experimental setup shown in Fig. 6(a), these system power loss values are directly obtained from the readings of the DC power source. The power loss measured in air environment is denoted as P_{air}. Particularly, P_{air} is a reference point, and it is attributed to the inverter loss P_{inv} and conductive passive loss P_{LC} in the solenoid coil and capacitors.

C. *Seven Tested Pavement Materials*

Based on the theoretical analysis of the uniform magnetic field from the section above. An *LCR* resonant circuit is established to resonate with the solenoid coil and generate the uniform magnetic field. The experimental platform is shown in Fig. 6(a). A full-bridge inverter provides ac power to the solenoid coil. Seven different pavement materials are tested, as shown in Table 1 and Fig. 6(b).

In this study, four types of concrete are tested, including 1) traditional Portland cement (PC) concrete, 2) granulated blast furnace steel slag (GBFS) modified concrete, 3) metakaolin (MK) modified concrete, and 4) fly ash (FA) modified concrete. Symbols representing the different concrete materials are

Table 1. Seven Tested Pavement Materials

Material	Key Components	Symbol
Concrete 1	traditional Portland cement (PC)	PC
Concrete 2	granulated blast furnace steel slag (GBFS) modified concrete	GBFS
Concrete 3	metakaolin (MK) modified concrete	MK
Concrete 4	fly ash (FA) modified concrete	FA
Asphalt 1	hot mix asphalt (HMA) nominal maximum aggregate size of 4.75 mm	HMA-4.75mm
Asphalt 2	hot mix asphalt (HMA) nominal maximum aggregate size of 9.5 mm	HMA-9.5mm
Asphalt 3	stone matrix asphalt (SMA) nominal maximum aggregate size of 12.5 mm	SMA-12.5mm

provided in Table 1. It is noted that GBFS, MK, and FA are porous materials with approximate air voids of 20%.

Among the 4 cement concrete specimens, PC is conventional concrete without any additives. GBFS, MK, and FA are porous cement concrete materials with many air voids within the material reducing water runoffs and allowing air and groundwater recharge. The variations of their colors are due to different types of additives. Each additive in GBFS, MK, and FA could provide various benefits such, increased strength and faster curing. More detailed information can be found in the authors' previous work of Ref. [35].

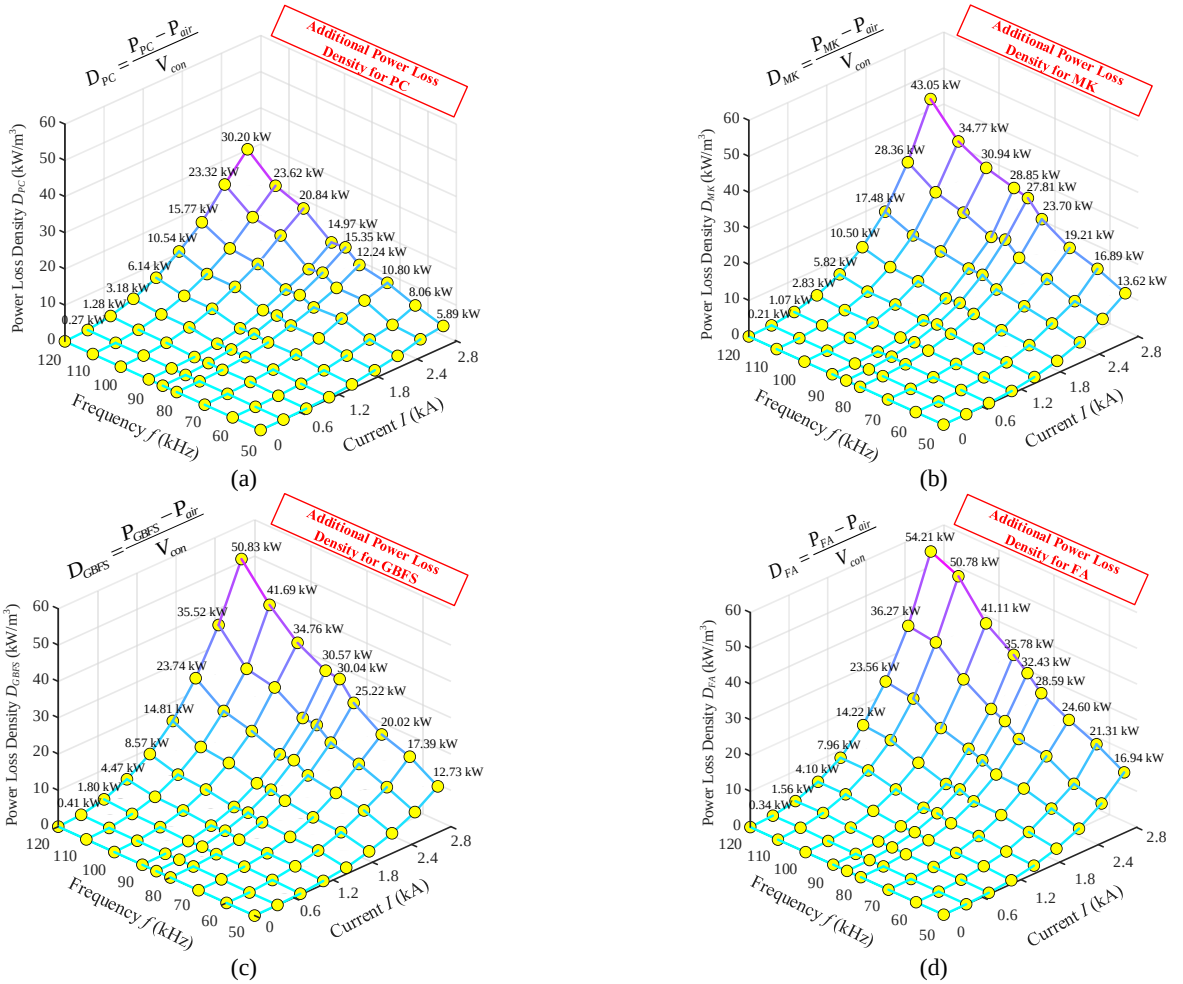

Fig. 7. Measured power loss density in concrete cement materials at various frequencies (50-120 kHz) and excitation current magnitudes (0-2.8 kA) in an implemented solenoid coil to quantify pavement impacts in a uniform magnetic field, showing FA concrete has the highest power loss. (a) Power loss density in concrete PC, maximum is 30.20 kW/m^3. (b) Power loss density in concrete MK, maximum is 43.05 kW/m^3. (c) Power loss density in concrete GBFS, maximum is 50.83 kW/m^3. (d) Power loss density in concrete FA, maximum is 54.21 kW/m^3.

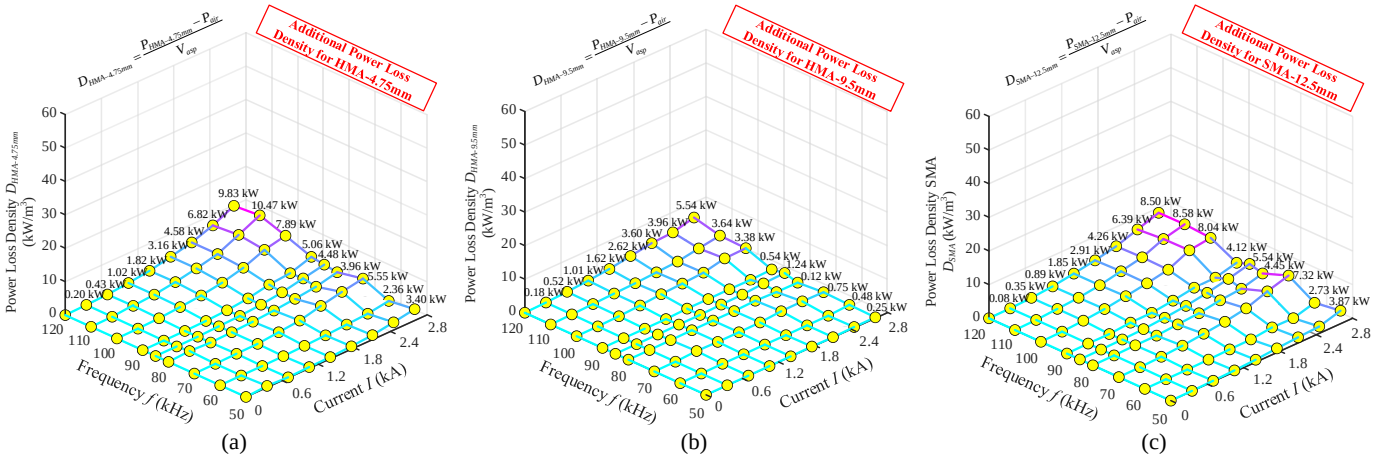

Fig. 8. Measured power loss density in asphalt materials at various frequencies (50-120 kHz) and excitation current magnitudes (0-2.8 kA) in an implemented solenoid coil to quantify pavement impacts in a uniform magnetic field, showing all asphalt materials have low power loss. (a) Power loss density in asphalt HMA-4.75mm. (b) Power loss density in asphalt HMA-9.5mm. (c) Power loss density in asphalt SMA-12.5mm.

For asphalt material, the dense-graded hot mix asphalt (HMA) mixture with nominal maximum aggregate size (NMAS) of 4.75 mm and 9.5 mm are used, which are labeled as HMA-4.75mm and HMA-9.5mm in Table 1. Dense-graded structure refers to a tightly packed structure for all the aggregate particles, such as the stone, sand, and gravel within the asphalt. It indicates fewer air voids between the aggregate particles resulting in a finer material texture.

In addition, gap-graded stone matrix asphalt (SMA) with NMAS of 12.5 mm is also tested, which is labeled as SM-12.5mm. Gap-graded structure refers to certain sizes of aggregate particles that are missing creating more air voids or gaps within the asphalt. SMA uses the largest size of aggregate particles that results the most of gaps in the material. More detailed information of the asphalt materials can be found in the authors' previous work of Ref. [36].

D. Quantifying the Impact Factors of Magnetic Loss

The pavement materials are tested inside the solenoid coil where the strong and uniform magnetic fields are present. Under this situation, the magnetic loss P_M, typically include eddy current loss P_{edd} and dielectric loss P_{die} [37], [38]. Based on a modified Steinmetz Equation model (5), these two types of loss are directly related to strength of magnetic flux density B, its alternating frequency f, and the material volume V.

$$P_M = P_{die} + P_{edd} = \int k_p f^{\beta} B^{\alpha} dV \tag{5}$$

In the equation, k_p is the material coefficient, which is mainly related to physical characteristics of pavement materials, such as their permeability, permittivity, and conductivity. For a given magnetic flux density B and its alternating frequency f, α and β are their coefficient respectively. Based on the analysis, it is assumed that all the material coefficients k_p, α and β are independent of each other.

To precisely determine the exact power loss under each combination of the above impact factors is difficult through an analytical method. Therefore, this experimental study is set up to directly collect and test the power loss data of various pavement materials within different uniform magnetic fields produced by the solenoid coil. Those tests results are subsequently analyzed through a rigorous statistical modeling to derive the parameter coefficients α, β, and k_p shown in (5).

E. Power Loss Density of Concrete Cement and Asphalt Specimens

In the power loss test, the 4 concrete cement specimens have the same volume V_{con}= 1.57 L, the 3 asphalt specimens have the same volume V_{asp}= 0.95 L. The power losses in the tested materials are respectively denoted as P_{PC}, P_{GBFS}, P_{MK}, and P_{FA}, $P_{HMA\text{-}4.75mm}$, $P_{HMA\text{-}9.5mm}$, and $P_{SMA\text{-}12.5mm}$.

When the transmitter of an IPT system is embedded in different pavement materials, the total system power loss P_{tot} includes P_{air} and the power loss for the given material. For example, the total system loss P_{tot} for concrete cement FA, which demonstrated the highest power loss, is represented in the Equation (6).

$$P_{tot} = P_{inv} + P_{LC} + P_M = P_{Air} + P_M \tag{6}$$

At any given frequency f, or magnetic flux density B, additional power loss is observed for each of all the 7 types of pavement materials and compared to P_{air}.

Furthermore, the power loss density D is calculated for each of the concrete cement and asphalt specimens, denoted as D_{PC}, D_{GBFS}, D_{MK}, D_{FA}, $D_{HMA\text{-}4.75mm}$, $D_{HMA\text{-}9.5mm}$, $D_{SMA\text{-}12.5mm}$. respectively. They are introduced to represent the loss power caused by the materials is shown in kilowatt per cubic meter (kW/m^3). For example, the power loss density for FA is defined in Equation (7) as D_{FA}.

$$D_{FA} = \frac{P_{tot} - P_{Air}}{V_{con}} = \frac{P_{FA}}{V_{con}} \tag{7}$$

Therefore, the power loss density for each of materials is calculated using equation similarly. The results for the 4 concrete cement specimens are shown in Fig. 7(a), (b), (c), and (d), and the power loss density for the 3 asphalt specimens are provided in Fig. 8(a), (b) and (c).

Fig. 7 demonstrated that as both frequency f and magnetic flux density B increases, the power loss density D of 4 concrete cement specimens increases dramatically compared with the 3 asphalt materials.

For the 4 concrete cement specimens, there is a positive correlation for the power loss density D with frequency f and magnetic field B. In particular, D is more sensitive to the increasing magnetic field B rather than the change in frequency f in all the combinations of the test conditions.

Among the tested concrete specimens, FA exhibits the highest power loss density in all tested frequencies when the excitation current for given magnetic flux density is higher than 2 kA. However, at excitation currents below 2 kA and specifically at 120 kHz, GBFS demonstrated higher power loss. In contrast, specimen PC consistently maintained the lowest power loss density under all experimental conditions.

Notably, with an excitation current I of 2.8 kA at 120 kHz, D_{FA} is 54.21 kW/m^3, significantly surpassing D_{PC} (30.20 kW/m^3) by over 44%. This significant variances in power loss density among different concrete specimens highlight the need for optimized pavement material selections to enhance efficiency and mitigate potential power loss in IPT systems operating with concrete specimens as the power transfer medium.

In Fig.8, all the power loss densities of asphalt show a trend similar to concrete cement specimens but on a smaller scale and with a less distinct correlation. Particularly, HMA-9.5mm shows little to no variation in loss density across all tested frequencies and magnetic flux densities, while HMA-4.75mm and SMA-12.5mm display higher power loss densities.

The asphalt materials do not clearly establish a positive correlation between their power loss densities and the magnetic field B or frequency f. Although the power loss densities for all asphalt are significantly lower than concrete cement specimens, the difference between the highest $D_{HMA\text{-}4.75mm}$ and the lowest $D_{HMA\text{-}9.5mm}$ is still over 43%, indicating a notable variance in power loss densities among all tested asphalt materials. These tests results are valuable for evaluating and selecting pavement materials for road construction and many other implications when we have pavement materials as the transfer medium.

Overall, asphalt materials demonstrate significantly lower power loss density for given frequency f and magnetic flux density B. Within concrete cement specimens, FA demonstrates overall highest power loss, and D_{PC} is the lowest among all concrete materials, but it is still much higher than the highest $D_{HMA\text{-}4.75mm}$ within the asphalt materials.

The results also reveal that asphalt materials, such as HMA-9.5mm, show the lowest power loss density compared to concrete materials. This makes asphalt a favorable option for embedding IPT systems, particularly in DWPT applications where minimizing power loss is crucial, such as high-power and high-frequency WPT systems. For concrete materials, PC exhibits the lowest D among all tested specimens and remains competitive with asphalt in terms of power loss density, making it a suitable candidate for IPT systems requiring high mechanical strength and durability. Although exact explanations for variations in D between FA and PC materials are complex, the experimental findings offer valuable insights into material selection for optimizing WPT system performance. The comprehensive experimental data collected, including the developed empirical model based on the modified Steinmetz Equation, enables a practical assessment of material suitability for different IPT applications.

Therefore, materials that have the lowest power loss density can be used to embed the transmitter of an IPT system. It is the HMA-9.5mm in the asphalt material group and PC in the concrete cement group. These two materials are further selected to be tested in an implemented IPT setup in Section IV.

III. Derive Empirical Equations of Material Loss

A. Case Study Example: Derive Power Loss Equation for Concrete Cement PC

Based on the *LCR* experimental setup in Fig. 6(a), all 7 pavement materials are tested under various magnetic fields B at different frequencies f. A coefficient k_p is proposed to describe the material's power loss characteristic. k_p is a coefficient determined by the materials themselves, which is relatively independent of the magnetic flux density B and the frequency f. In addition, the magnetic field coefficient α and the frequency coefficient β are also proposed to represent the power loss density D, as shown in Equation (8).

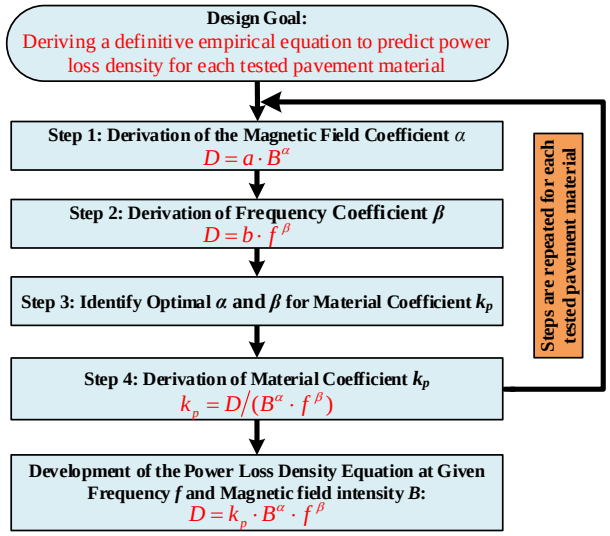

Fig. 9. Flow chart of the proposed derivation procedure of empirical equation of power loss in pavement materials, including the magnetic field coefficient α, frequency coefficient β, and material coefficient k_p.

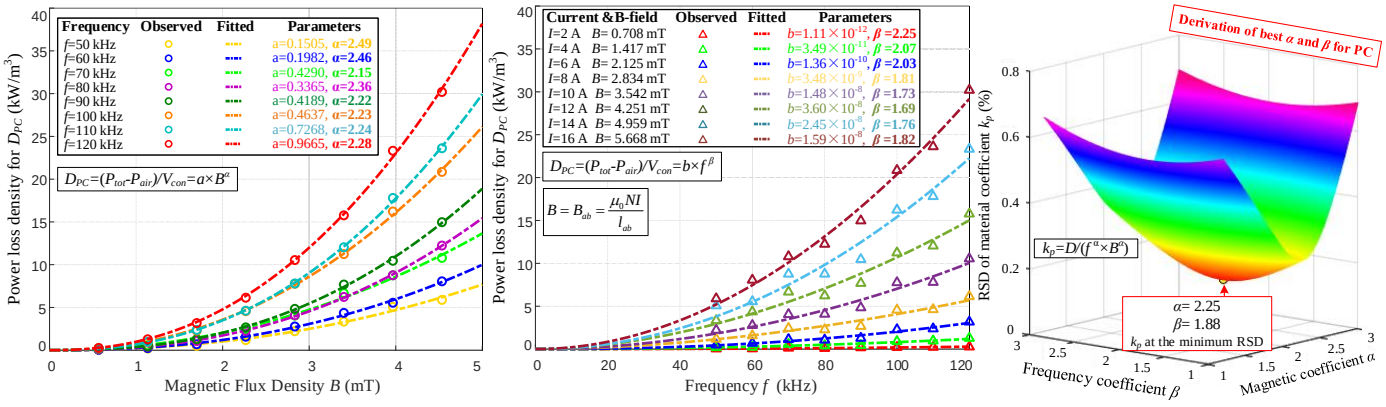

Fig.10. The statistical derivation of the impact parameters in an empirical equation to model the power loss density D of concrete cement PC at various magnetic flux densities (0-5 mT) and frequencies (0-120 kHz). a) Derivation of magnetic field coefficient α. b) Derivation of frequency coefficient β. (c) Identify optimal α, β for deriving of k_p.

TABLE. 2. EMPIRICAL EQUATIONS OF PAVEMENT MATERIALS

Material Name	k_p	α	β	Derived Empirical Equation	Predicted D (kW/m³) At 85kHz	Observed D (kW/m³) At 85kHz	Average Accuracy
PC	8.45184×10^{-4}	2.25	1.88	D= $8.45184\times10^{-4}B^{2.25}\cdot f^{1.88}$	0.129~13.316	0.113~15.350	91.77%
GBFS	1.14819×10^{-1}	2.36	1.56	D= $1.14819\times10^{-1}B^{2.36}\cdot f^{1.56}$	0.287~30.038	0.207~28.049	89.30%
MK	3.39149	2.48	1.315	D= $3.39149B^{2.48}\cdot f^{1.315}$	0.247~27.809	0.159~27.605	86.16%
FA	7.27544×10^{-2}	2.45	1.64	D= $7.27544\times10^{-2}B^{2.45}\cdot f^{1.64}$	0.170~27.664	0.170~32.433	93.11%
SMA-12.5mm	1.17454×10^{-1}	2.02	1.275	D= $1.17454\times10^{-1}B^{2.02}\cdot f^{1.275}$	0.098~6.557	0.055~9.215	70.77%
HMA-4.75mm	5.67358×10^{-4}	1.595	1.5	D=$5.67358\times10^{-4}B^{1.595}\cdot f^{1.5}$	0.133~3.670	0.535~7.455	66.45%
HMA-9.5mm	1.13023×10^{-3}	1.63	1.36	D=$1.13023\times10^{-3}B^{1.63}\cdot f^{1.36}$	0.042~1.245	0.019~2.057	51.42%

$$D = k_p \cdot B^{\alpha} \cdot f^{\beta} \tag{8}$$

The target of this section is to utilize the concrete cement PC as an example to derive the empirical equation of power loss in

pavement materials. The proposed derivative procedures are shown in Fig. 9.

At a given frequency *f*, the power loss density *D* can be decoupled, as shown in Equation (9), to simplify the process of the statistical modeling.

$$D = a \cdot B^{\alpha} \tag{9}$$

Fig. 10(a) shows the derivation for each α at the tested frequency *f* with respect to the change of magnetic field *B* for concrete cement PC.

The same analytical process can also be applied to derive the frequency coefficient β as shown in Equation (10). Fig. 10(b) displays the analysis results of concrete cement PC, charting how each β at the tested magnetic field *B* with respect to the change of frequency *f*.

$$D = b \cdot f^{\beta} \tag{10}$$

The material coefficient k_p can be derived using Equation (11) with various experimental conditions of *B* and *f*.

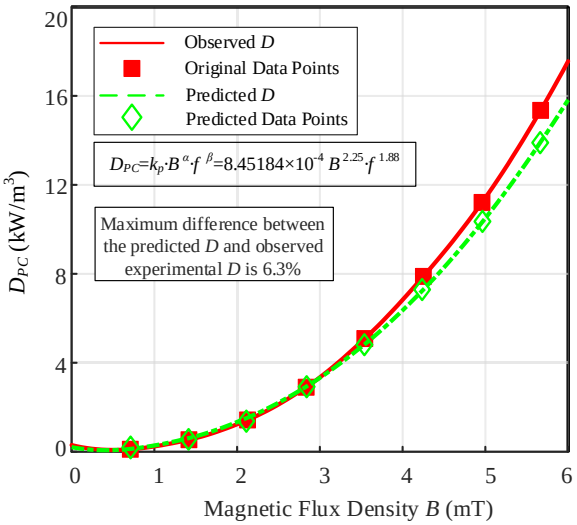

Fig. 11. Predicted vs. observed power loss density *D* for concrete cement PC at *f*=85 kHz with an average accuracy of 91.77% across magnetic flux densities *B* (0-5 mT).

$$k_p = \frac{D}{B^{\alpha} \cdot f^{\beta}} \tag{11}$$

Optimal values of α and β are determined by Equation (11) as shown in Fig. 10(c). The RSD of the calculated k_p across all combination of α and β for concrete cement PC. The lowest RSD of k_p is achieved at α=2.25 and β=1.88.

The material coefficient k_p can be quantified with the optimal α=2.25 and β=1.88 for concrete cement PC. Fig. 11 presents a comparison between the predicted power loss density *D* using the developed empirical equation, and the observed *D* from the experiments.

This comparison demonstrates the accuracy of the prediction model across various magnetic flux densities *B* at *f*=85 kHz. For instance, the average accuracy of concrete cement PC for predicting the *D* using the derived empirical equation is at 91.77% with maximum accuracy at 99.17% and minimum accuracy at 85.20% for all the compared data sets.

$$D_{PC} = 8.54184\times10^{-4} \cdot B^{2.25} \cdot f^{1.88} \tag{12}$$

The definitive empirical equation (12) quantities the power loss density *D* in the concrete cement specimen PC. Therefore, the development of this predictive equation for quantifying system power loss contributes significantly to the advancement and optimization of the design and implementation of road embedded IPT system for EV charging.

B. Identify Empirical Equations for All Tested Materials.

The material coefficient k_p, the magnetic field coefficient α and the frequency coefficient β are derived for all pavement materials using the procedure described in the flow chart in Fig. 9. The empirical equations are summarized in Table 2.

The average accuracy of predictions for concrete cement specimens is generally higher than that for asphalt materials, attributable to the greater power loss densities observed in the experiments. Since the power loss densities for all asphalt materials fall within the single digits in terms of kilowatts per cubic meter (kW/m³), when potential experimental errors are considered, the relative standard deviations (RSD) for these materials are higher than desired. Consequently, the average accuracy in predicting the power loss density for asphalt materials is relatively low.

IV. Inductive Power Transfer System to Test the Pavement Material Power Loss

A. An Experimental IPT Testing Prototype

Fig. 12 (a) illustrates the proposed 85 kHz/17.8 kHz IPT testing prototype, which is configurated as a series-series compensation as provided in the circuit schematic of Fig. 12(b). V_{dc} is the input dc voltage and V_{out} is output voltage at the rectifier. The IPT system is tuned to resonance at 85 kHz delivered by a full bridge inverter using four Wolfspeed C3M0016120K SiC MOSFETs, which are rated for 1200 V and 115 A with a low on-state resistance of 16 mΩ. A TMS320F28335 microcontroller is used to generate the 85kHz drive signal. At the receiving side, a low loss SiC based full bridge rectifier is connected. The rectifier design employs the Infineon IDW30G65C5 SiC Schottky diodes, which are rated for 650 V and 30 A. An eight-channel Tektronix 5 Series oscilloscope is used to collect waveform data, and a Yokogawa WT1806E precision power analyzer is used to measure power DC-DC power and efficiency.

The Tx and Rx coils are compensated by series capacitors C_{Tx} = 14.26 nF and C_{Rx} =14.16 nF. The system employes a transmitter and a receiver, L_{Tx}= 248 μH and L_{Rx}=247 μH with ferrite bars. The quality factor of transmitter coil and receiver coil is Q_{Tx}= 354.5 and Q_{Rx}= 369.6 respectively. The air gap between Tx and Rx coils is set at 175 mm, which closely aligns with industry standards for EV wireless charging. This gap falls within the 100 mm to 200 mm air gap range specified by the J2954 standards. The coupling coefficient *k* is 0.13.

As demonstrated in the circuit schematic in Fig. 12(b), the power recirculation setup allows the rectified DC output from the Rx coil to be fed back into the DC input source, creating a closed-loop configuration. This configuration enables the system to effectively recycle power between the Tx and Rx coils, achieving higher power levels in a controlled laboratory setting without the need for an external high-power load [39],

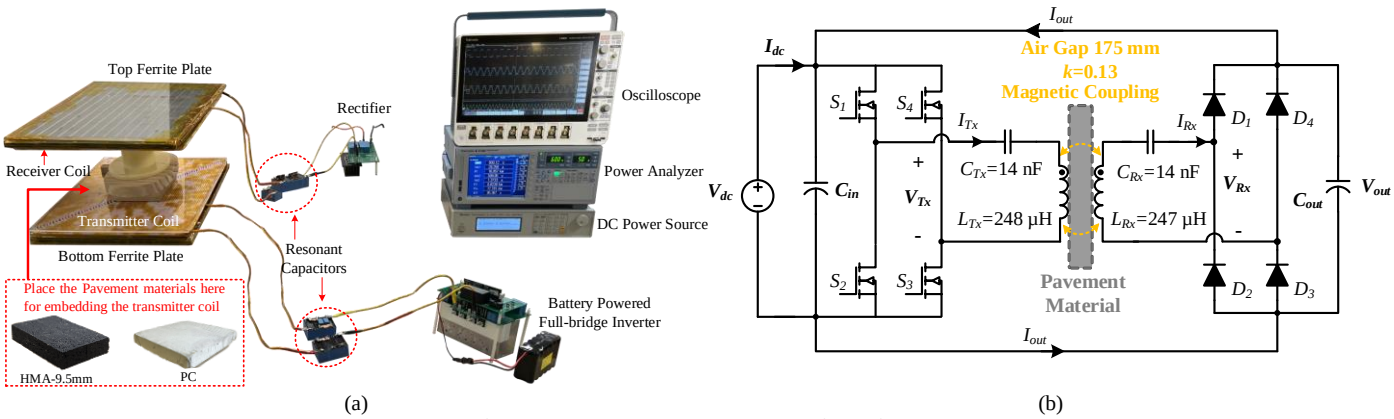

Fig. 12. Experimental IPT prototype to test the impact of pavement materials to the power transfer performance. (a) Proposed 18-kW IPT experimental setup. (b) S-S compensated circuit topology with power recycling capability.

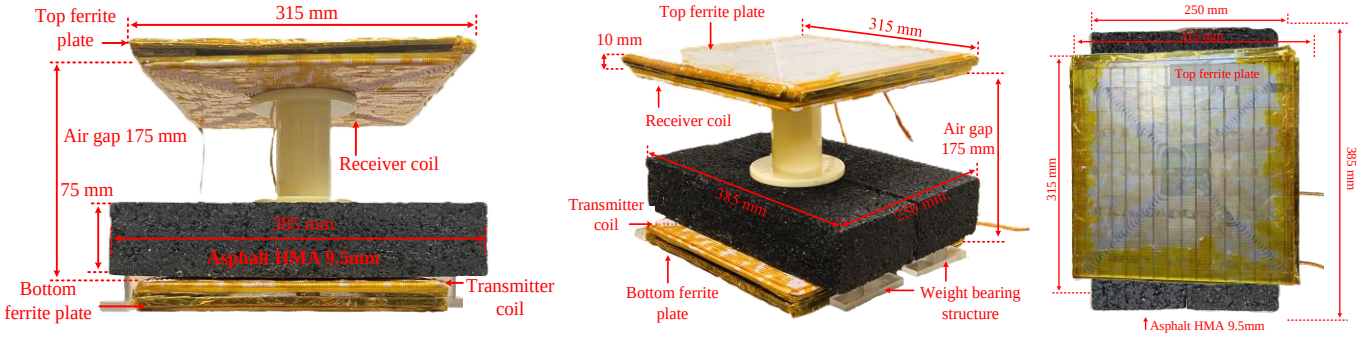

Fig. 13. IPT experimental coil structure for asphalt HMA-9.5mm (500 mm×400 mm×50 mm) as the medium. This setup mimics a transmitter coil embedded in 50 mm beneath the material to measure power loss density across a range of input power (0.5-17.172 kW). (a) Front view. (b) Isometric view. (c) Top view.

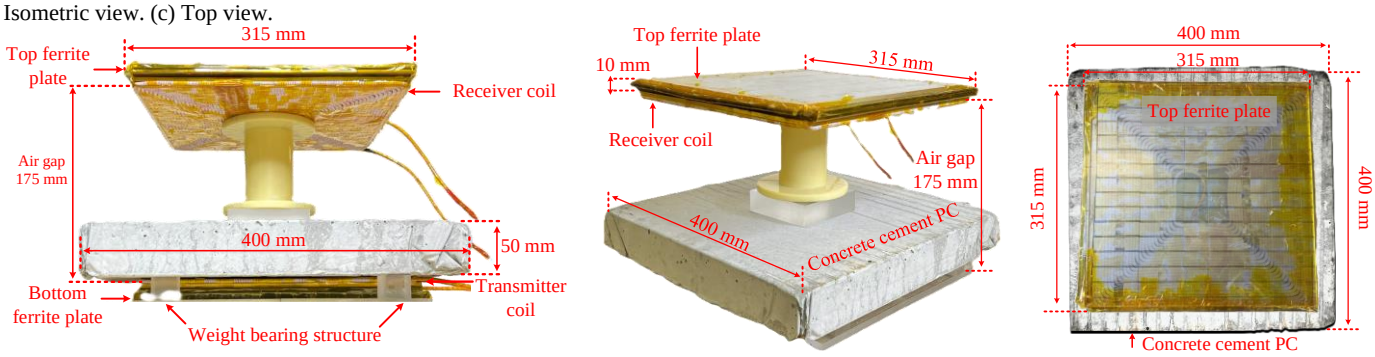

Fig.14. IPT experimental coil structure featuring concrete cement PC as the medium (400 mm×400 mm×50 mm), mimicking a transmitter coil embedded 50 mm beneath the material to measure power loss density across various input power (0.5-17.833 kW). (a) Front view. (b) Isometric view. (c) Top view.

[40]. The P_{loss} can be directly measured using the DC power source, as it only needs to supply power to offset the system losses rather than the full operational power. This setup simplifies the assessment of system efficiency, as the observed power loss accurately reflects the system's overall performance under various test conditions.

Both the Tx and Rx coils are constricted using 800 strands litz wire with 0.1 mm diameter for each strand. The dimensions for transmitter and receiver coils are 300 mm×300 mm×5 mm with a total of 28 turns as demonstrated in Fig. 3(a) in Section II. for the coil structure of the proposed IPT system. The pavement materials are placed between coils, and they tested individually under various conditions with different magnetic field B under frequency f=85 kHz.

The maximum power transfer efficiency when using only air as the transfer medium can be calculated using Ref. [41]. In an ideal scenario for implementing an IPT system for wireless EV charging, the road pavement material exhibiting the lowest power loss density D should be selected for embedding the transmitter coil. This choice minimizes undesired additional power loss and enhances the overall system efficiency.

Therefore, considering the 3 tested asphalt materials, HMA-9.5mm is selected to reduce power loss. Also, considering the 4 tested concrete cement specimens, PC is chosen. Both selected pavement materials exhibit the lowest power loss density D within their respective material groups, under the uniform magnetic field generated by the solenoid coil test.

Given these findings, it is crucial to further investigate the power loss density D for the selected pavement material specimens, HMA-9.5mm and PC, under the proposed practical

IPT system setup as shown in Fig. 12(a).

B. HMA-9.5mm and PC Materials Between Coils

Fig.13 and Fig. 14 illustrate the experimental coil structures for the proposed IPT prototype with asphalt HMA-9.5mm and concrete cement PC as the materials to embed the transmitter coil. Both materials are formed into block shapes with dimensions of 385 mm×250 mm×75 mm for HMA-9.5mm, and 400 mm ×400 mm×50 mm for PC.

The volumes for the HMA-9.5mm and concrete cement PC are V_a=10 L and V_c= 7.22 L respectively. Their volumes are used to calculate the power loss density for each material. To ensure an accurate measurement of the additional magnetic loss caused by materials, they are placed at the center of the Tx and Rx coils.

In a particle IPT charging system for EVs, the transmitter coil is encased in a protective package to reinforce its durability and withstand the exerted by the pavement material and weight of the vehicles. Given the substantial size and weight of both materials, exceeding 20 kg each, a weight-bearing structure is implemented to manage the pressure exerted by the materials.

This structure is essential for mitigating the impact on the embedded transmitter coil, preserving its structural and functional integrity to simulate a real IPT charging system in particle applications.

Ferrite plates are utilized for both the transmitter and receiver coils. Their dimensions measure at 315 mm×315 mm×10 mm, slightly larger than the coils themselves, to increase inductance and concentrate the magnetic fields effectively. The air gap for testing both materials is consistently maintained at 175 mm throughout the experiment, ensuring a steady magnetic coupling coefficient k=0.13.

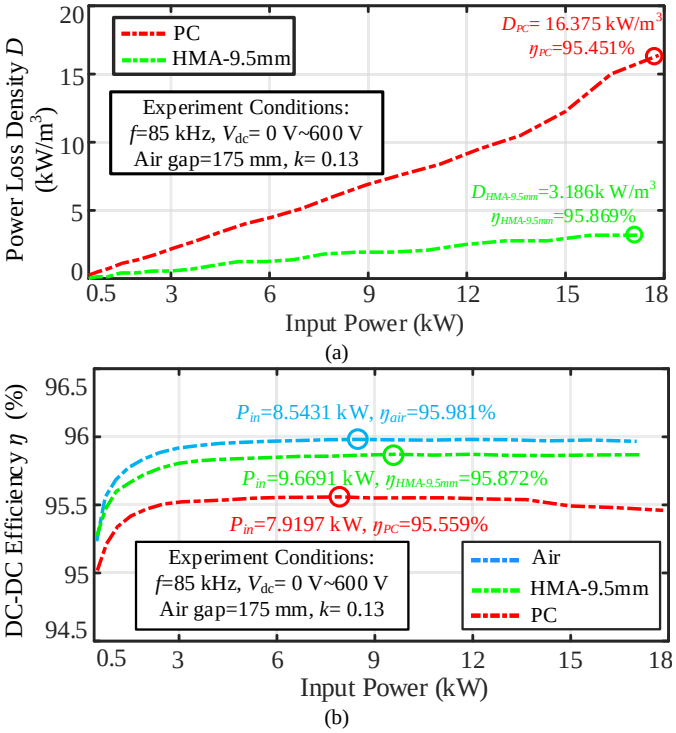

Fig. 15. IPT system experimental results when using the selected asphalt and concrete as transfer medium and compared with the air environment. (a) Power loss density of HMA-9.5mm asphalt and PC concrete. (b) Efficiency with air, HMA-9.5mm, and PC as medium.

C. Power Loss Density of Pavement Materials in IPT System

Fig. 15(a) shows the power loss density D for each of these two pavement materials across a range of input power from 0.5 kW to 17.833 kW at frequency f=85 kHz. At the maximum input power P_{in}=17.172 kW, the HMA-9.5mm demonstrates the power loss density $D_{HMA\text{-}9.5mm}$=3.186 kW/m^3 with system efficiency at 95.869%. For PC, the power loss density

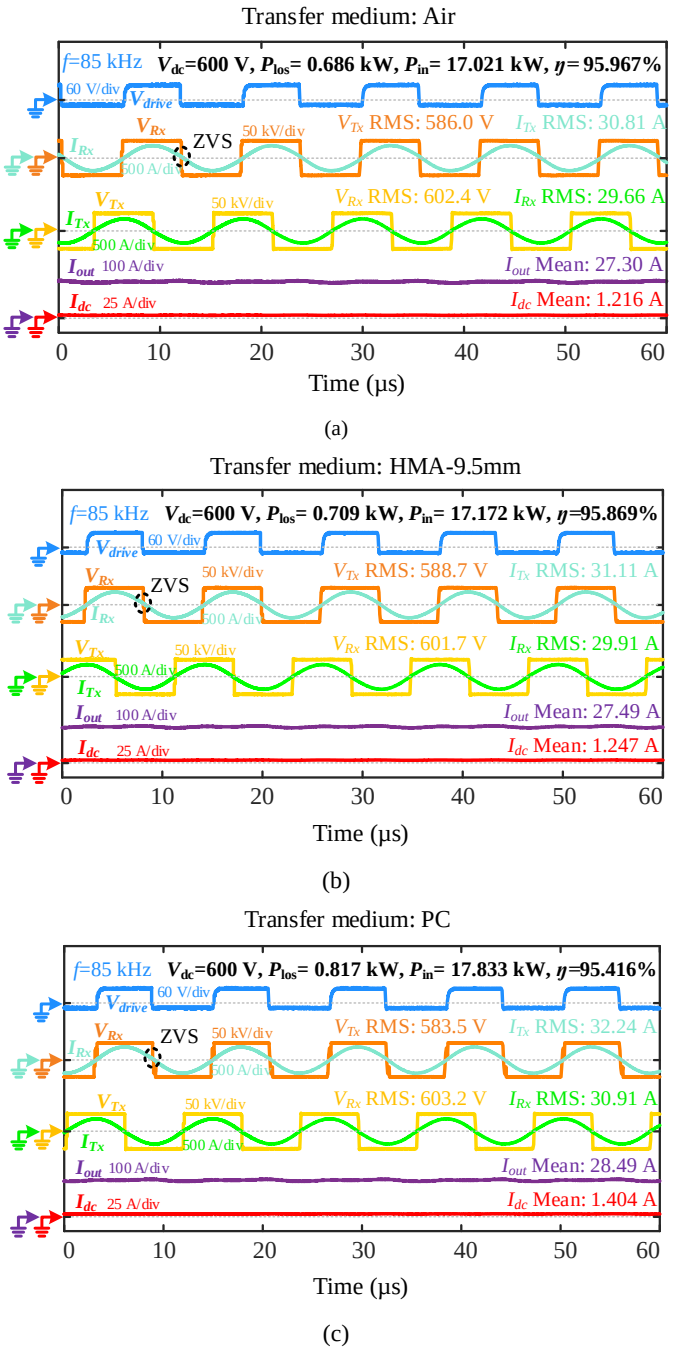

Fig. 16. Experimental waveforms and measurement results of critical voltages and currents when pavement materials exist between coils. (a) No pavement materials between coils (air). (b) HMA-9.5mm asphalt material between coils. (c) PC concrete material between coils.

D_{PC}=16.375 kW/m^3 and the system efficiency is 95.451%.

The DC-DC system efficiencies of the implemented IPT system, which uses air, asphalt material HMA-9.5mm, and

concrete cement PC as the power transfer medium, are detailed in Fig. 15(b). The peak efficiencies achieved for those 3 mediums are η_{air}=95.981% with an input power of 8.543 kW, $\eta_{HMA\text{-}9.5mm}$=95.872% when the input power is at 9.669 kW, and η_{PC}=95.559% when P_{in}=7.919 kW respectively. When compared to η_{air}, the efficiencies for both materials are lower due to additional power loss incurred by the pavement materials.

The experimental waveforms are provided in Fig. 16. With f=85 kHz, V_{dc}=600 V. The performance of the implemented IPT system is investigated with air, asphalt material HMA-9.5mm, and concrete cement PC.

Fig. 16 (a) shows the maximum input power P_{in}=17.021 kW with DC-DC peak system efficiency of 95.967% when air is used as the transfer medium in the well-aligned condition. The system power loss can be directly observed and calculated using the V_{dc} and I_{dc} readings from the dc power source, since the power circulates between the Tx and Rx coils and the power supply only provides additional power loss for the experiment. The slight phase shift between V_{Tx} and V_{Rx} is intentionally designed into the experiment aiming at achieving zero-voltage switching (ZVS).

With asphalt material HMA-9.5mm and concrete cement PC as the power transfer mediums, Figs. 16 (b) and (c) respectively display the experimental waveforms. For HMA-9.5mm, the maximum P_{in}=17.172 kW, and for PC, the maximum P_{in} is 17.833 kW, both in the well-aligned condition. The power loss P_{loss} is 0.709 kW for HMA-9.5mm and 0.817 kW for PC when V_{dc}=600 V at their respective system maximum input power.

V. Conclusion

This study investigates the power loss characteristics of seven different roadway pavement materials when used as the power transfer medium in IPT systems for EV charging. The research provides a detailed analysis of power loss density D under various combinations of magnetic flux density B from 0 mT to over 7 mT and frequency f from 50 kHz to 120 kHz using a solenoid coil setup. Based on the experimental data, empirical equations were developed to quantify material-specific power loss characteristics, enabling a more precise understanding of material behavior in IPT systems.

The study highlights the significant variations in power loss density among different pavement materials, particularly between concrete cement and asphalt specimens. Concrete materials, such as FA, exhibited the highest power loss densities under tested conditions, whereas asphalt materials showed comparatively lower losses, making them more suitable for minimizing energy dissipation in IPT applications.

A modified Steinmetz Equation model was proposed to describe the power loss behavior of pavement materials. This model, validated through extensive experimental data, offers a reliable method to predict power loss based on material properties, magnetic flux density, and frequency. The derived parameter coefficients and predictive accuracy for each material are displayed in Table 2.

The research identified that PC in the concrete group and HMA-9.5mm in the asphalt group demonstrated the lowest power loss densities, making them ideal candidates for embedding IPT system transmitters. These findings are crucial for optimizing IPT system design, especially for applications that require high efficiency and minimal power loss. The final stage of the study involved implementing a 17.8 kW/85 kHz series-series IPT prototype to test the selected materials. The results confirmed that HMA-9.5mm and PC maintained their low power loss characteristics in a practical IPT setup, with power loss densities of $D_{HMA\text{-}9.5mm}$=3.186 kW/m^3 and D_{PC}=16.375 kW/m^3 respectively. These values highlight the material's impact on overall system performance and provide practical guidance for material selection in real-world IPT applications.

Therefore, this research offers valuable insights into the selection and application of pavement materials in IPT systems, providing a foundation for further optimization and implementation of efficient wireless EV charging infrastructure.

References

[1] O. Kaiwartya et al., "Internet of Vehicles: Motivation, Layered Architecture, Network Model, Challenges, and Future Aspects," in *IEEE Access*, vol. 4, pp. 5356-5373, 2016.

[2] U. B S, V. Khadkikar, H. H. Zeineldin, S. Singh, H. Otrok and R. Mizouni, "Direct Electric Vehicle to Vehicle (V2V) Power Transfer Using On-Board Drivetrain and Motor Windings," in *IEEE Trans. on Ind. Electron.*, vol. 69, no. 11, pp. 10765-10775, Nov. 2022.

[3] A. Zakerian, S. Vaez-Zadeh and A. Babaki, "A Dynamic WPT System With High Efficiency and High Power Factor for Electric Vehicles," in *IEEE Trans. on Power Electron.*, vol. 35, no. 7, pp. 6732-6740, July 2020.

[4] H. Zhou, Z. Shen, Y. Wu, X. Chen and Y. Zhang, "A Stable Dynamic Electric Vehicle Wireless Charging System Based on Triple Decoupling Receiving Coils and a Novel Triple-Diode Rectifier," in *IEEE Transactions on Industrial Electronics*, vol. 71, no. 10, pp. 12011-12018, Oct. 2024.

[5] Y. Li et al., "A New Coil Structure and Its Optimization Design With Constant Output Voltage and Constant Output Current for Electric Vehicle Dynamic Wireless Charging," in *IEEE Trans. on Ind. Inform.*, vol. 15, no. 9, pp. 5244-5256, Sept. 2019.

[6] V. Cirimele, M. Diana, F. Freschi and M. Mitolo, "Inductive Power Transfer for Automotive Applications: State-of-the-Art and Future Trends," in *IEEE Transactions on Industry Applications*, vol. 54, no. 5, pp. 4069-4079, Sept.-Oct. 2018.

[7] H. Zhou, Z. Shen, Y. Wu, X. Chen and Y. Zhang, "A Stable Dynamic Electric Vehicle Wireless Charging System Based on Triple Decoupling Receiving Coils and a Novel Triple-Diode Rectifier," in *IEEE Transactions on Industrial Electronics*, vol. 71, no. 10, pp. 12011-12018, Oct. 2024.

[8] S. Jeong, Y. J. Jang and D. Kum, "Economic Analysis of the Dynamic Charging Electric Vehicle," in *IEEE Transactions on Power Electronics*, vol. 30, no. 11, pp. 6368-6377, Nov. 2015.

[9] Bombardier PRIMOVE Website. [Online]. Available: http://primove. bombardier.com/media/news/, accessed Dec. 2013.

[10] C. C. Mi, G. Buja, S. Y. Choi and C. T. Rim, "Modern Advances in Wireless Power Transfer Systems for Roadway Powered Electric Vehicles," in *IEEE Transactions on Industrial Electronics*, vol. 63, no. 10, pp. 6533-6545, Oct. 2016.

[11] Z. Bingke and L. Jingyun, "A review of research on wireless charging technology for electric vehicles," *2023 26th International Conference on Electrical Machines and Systems (ICEMS)*, Zhuhai, China, 2023, pp. 4791-4797.

[12] Z. Bi, T. Kan, C. C. Mi, Y. Zhang, Z. Zhao, and G. A. Keoleian, "A review of wireless power transfer for electric vehicles: Prospects to enhance sustainable mobility," Appl. Energy, vol. 179, pp. 413–425, Oct. 2016.

[13] S Laporte, G. Coquery, V. Deniau, A. De Bernardinis, and N Hautière, "Dynamic Wireless Power Transfer Charging Infrastructure for Future EVs: From Experimental Track to Real Circulated Roads Demonstrations," *World Electric Vehicle Journal*, vol 10, no. 4, pp 84, Nov. 2019.

[14] Y. Shanmugam *et al*., "A Systematic Review of Dynamic Wireless Charging System for Electric Transportation," in *IEEE Access*, vol. 10, pp. 133617-133642, 2022.

[15] Bozhi, M. Mohamed, V. Gilani, A. Amjad, M. Sh. Majid, K. Yahya, and M. Salem, "A Review of Wireless Pavement System Based on the Inductive Power Transfer in Electric Vehicles" *Sustainability*, vol. 15, no. 20, pp. 14893, Oct. 2023.

[16] R. Xie, Y. Wu, H. Tang, Y. Zhuang and Y. Zhang, "A Strongly Coupled Vehicle-to-Vehicle Wireless Charging System for Emergency Charging Purposes with Constant-Current and Constant-Voltage Charging Capabilities," in *IEEE Trans. on Power Electron.*, vol. 39, no. 4, pp. 3985-3989, April 2024.

[17] Y. Wang, A. Mostafa, Z. Zheng, H. Zhang, J. Zhu and F. Lu, "Highly Misalignment-Tolerant Series-Series IPT System with Overcurrent and Overpower Protection for Underwater Manta Ray Robots," *2023 IEEE Wireless Power Technology Conference and Expo (WPTCE)*, San Diego, CA, USA, 2023, pp. 1-6.

[18] V. Cirimele, F. Freschi and L. Zhao, "Critical Comparative Review of International Standards on Wireless Charging for Light-Duty Electric Vehicles," in *IEEE Transactions on Industry Applications*, vol. 60, no. 5, pp. 7403-7412, Sept.-Oct. 2024

[19] "Wireless Power Transfer for Light-Duty Plug-in/Electric Vehicles and Alignment Methodology", SAE J2954 202208, Society of Automotive Engineers, 2022.

[20] "Wireless Power Transfer for Heavy-Duty Electric Vehicles", SAE J2954/2 202212, Society of Automotive Engineers, 2022.

[21] A. Beeldens, P. Hauspie, and H. Perik, "Inductive charging through concrete roads: A Belgian case study and application," in *Proc. 1st Eur. Road Infrastruct. Congr.*, Leeds, U.K., 2016, pp. 1–10.

[22] R. Tavakoli et al., "Magnetizable concrete composite materials for road-embedded wireless power transfer pads," *2017 IEEE Energy Conversion Congress and Exposition (ECCE)*, Cincinnati, OH, USA, 2017.

[23] P. Aghcheghloo et al., "Evaluation of the behavior of the interface zone between an asphalt mixture and an inductive power transfer pad," *Construction and Building Materials*, vol. 411, pp. 134038, 2024.

[24] C. -H. Ou, H. Liang and W. Zhuang, "Investigating Wireless Charging and Mobility of Electric Vehicles on Electricity Market," *IEEE Trans. Ind. Electron.*, vol. 62, no. 5, pp. 3123-3133, May 2015.

[25] Z. Zheng et al., "Power Loss Investigation of Pavement Materials in Roadway Inductive Charging System," *2024 IEEE Applied Power Electronics Conference and Exposition (APEC)*, Long Beach, CA, USA, 2024, pp. 1905-1908.

[26] S. Jayalath and A. Khan, "Design, Challenges, and Trends of Inductive Power Transfer Couplers for Electric Vehicles: A Review," in *IEEE J. Emerg. Sel. Topics in Power Electron.*, vol. 9, no. 5, pp. 6196-6218, Oct. 2021.

[27] R. Tavakoli, E. M. Dede, C. Chou and Z. Pantic, "Cost-Efficiency Optimization of Ground Assemblies for Dynamic Wireless Charging of Electric Vehicles," in *IEEE Trans. on Trans. Electr.*, vol. 8, no. 1, pp. 734-751, March 2022.

[28] F. Chen, N. Taylor, R. Balieu, and N. Kringos, "Dynamic application of the inductive power transfer (IPT) systems in an electrified road: Dielectric power loss due to pavement materials," Construct. Building Mater., vol. 147, pp. 9–16, Aug. 2017.

[29] V. Cirimele, R. Torchio, A. Virgillito, F. Freschi, and P. Alotto, "Challenges in the electromagnetic modeling of road embedded wireless power transfer, Energies," vol. 12, no. 14, p. 2677, Jul. 2019.

[30] M. Amirpour, S. Kim, M. P. Battley, P. Kelly, S. Bickerton, and G. Covic, "Coupled electromagnetic-thermal analysis of roadway inductive power transfer pads within a model pavement," Appl. Thermal Eng., vol. 189, May 2021.

[31] R. Tavakoli *et al*., "Magnetizable concrete composite materials for road-embedded wireless power transfer pads,"*2017 IEEE Energy Conversion Congress and Exposition (ECCE)*, Cincinnati, OH, USA, 2017, pp. 4041-4048, doi: 10.1109/ECCE.2017.8096705.

[32] G. Blankson, M. Darwish and C. S. Lai, "Wireless Power Transfer System for Electric Vehicle Charging with Frequency Hopping – A Concept and Circuit Design," *2023 58th International Universities Power Engineering Conference (UPEC)*, Dublin, Ireland, 2023.

[33] Xia, N., Chen, M. & Zhu, Y. A Dynamic Wireless Charging System Based on Transmitter Module Composed of Coplanar Double Bipolar Pads with Hybrid Compensation Topology. *J. Electr. Eng. Technol.* 19, 1429–1438, 2024.

[34] W. Zhang and C. C. Mi, "Compensation topologies of high-power wireless power transfer systems," IEEE Transactions on Vehicular Technology, vol. 65, no. 6, pp. 4768–4778, 2015

[35] W. Huang, H. Wang, "Multi-aspect Engineering Properties and Sustainability Impacts of Geopolymer Pervious Concrete," Composites Part B: Engineering, vol. 242, pp. 110035, August 2022.

[36] X. Chen, H. Wang, B. Jiang, G. Venkiteela, "Evaluation of microwave heating for potential applications in hot in-place recycling of asphalt pavement", Transportation Research Record, vol. 2676, no. 9, pp. 256-268, April 2022.

[37] Y. Wang et al., "Experimental Investigation of the Eddy-Current and Dielectric Loss of Underwater IPT System," *2023 IEEE Energy Conversion Congress and Exposition (ECCE)*, Nashville, TN, USA, 2023.

[38] G. Novak, J. Kokošar, M. Bricelj, M. Bizjak, D. Steiner Petrovič and A. Nagode, "Improved Model Based on the Modified Steinmetz Equation for Predicting the Magnetic Losses in Non-Oriented Electrical Steels That is Valid for Elevated Temperatures and Frequencies," in *IEEE Trans. on Magnetics*, vol. 53, no. 10, pp. 1-5, Oct. 2017.

[39] A. Mostafa, Y. Wang, F. Lu, and H. Zhang, "Enhanced axial misalignment tolerance in a 10-kW autonomous underwater vehicle wireless charging system utilizing a split solenoid coupler," *IEEE Trans. Power Electron.*, vol. 39, no. 10, pp. 12041–12045, Oct. 2024.

[40] S. Lu, D. Kong, S. Xu, L. Luo, and S. Li, "A high-efficiency 80-kW split planar transformer for medium-voltage modular power conversion," *IEEE Trans. Power Electron.*, vol. 37, no. 8, pp. 8762–8765, Aug. 2022.

[41] S. Li and C. C. Mi, "Wireless power transfer for electric vehicle applications," *IEEE J. Emerg. Sel. Topics Power Electron.*, vol. 3, no. 1, pp. 4–17, Mar. 2015.

Manuscript received July 19, 2024; revised Oct. 02, 2024; revised Nov. 25, 2024; accepted Dec. 25, 2024. This work was supported by XXX program. *(Corresponding Author: Fei Lu)*

Zilong Zheng is with the Department of Electrical and Computer Engineering, Drexel University, Philadelphia, PA 19104, USA. (e-mail: zz529@drexel.edu)

Xiao Chen and Hao Wang are with the Department of Civil and Environmental Engineering at Rutgers, The State University of New Jersey, New Brunswick, NJ, 08901, USA. (e-mail: xc299@scarletmail.rutgers.edu; hw261@soe.rutgers.edu)

Yao Wang is with the School of Electrical and Electronic Engineering, Nanyang Technological University, Singapore, 639798, Singapore. (e-mail: yao.wang@ntu.edu.sg)

Fei Lu and Hua Zhang are with the Department of Electrical and Computer Engineering, Lehigh University, Bethlehem, PA 18015, USA. (e-mail: fel324@lehigh.edu; huz524@lehigh.edu)